Kineto-dynamic modeling of human upper limb for robotic manipulators and assistive applications

Giuseppe Averta, Gemma C. Bettelani, Cosimo Della Santina and Matteo Bianchi

Abstract The sensory-motor architecture of human upper limb and hand is characterized by a complex inter-relation of multiple elements, such as ligaments, muscles and joints. Nonetheless, humans are able to generate coordinated and meaningful motor actions to explore and interact with the external world. Such a complexity reduction is usually studied within the framework of synergistic control, whose focus has been mostly limited on human grasping and manipulation. Little attention has been devoted to the spatio-temporal characterization of human upper limb kinematic strategies and how the purposeful exploitation of the environmental constraints shapes human execution of manipulative actions. In this chapter, we report results on the evidence of a synergistic control of human upper limb and during manipulation with the environment. We propose functional analysis to characterize main spatio-temporal coordinated patterns of arm joints. Furthermore, we study how the environment influences human grasping synergies. The effect of cutaneous impairment is also evaluated. Applications to the design and control of robotic manipulation and assistive devices are finally discussed.

Key words: motor control, daily living activities, upper limb, functional analysis, human-inspired robotics

Giuseppe Averta, Gemma C. Bettelani, Cosimo Della Santina and Matteo Bianchi
Centro di Ricerca Enrico Piaggio, Universita di Pisa, Largo L. Lazzarino 1, 56122 Pisa, Italy
e-mail: giuseppe.averta@ing.unipi.it

1 Introduction

Human hands are our pre-eminent organ to interact with and manipulate the external environment. Its wonderful architecture gives humans a wide spectrum of possibilities, which can be roughly summarized in the four functional groups of sensation, holding, manipulation and communication. Despite the complexity of the biomechanics and the high versatility of the sensory-motor behavior it embeds, the human brain is able to cope with and organize it in a simple fashion [9], leveraging on a control space of reduced dimensionality [46, 54, 39, 62], usually defined as synergistic control space.

This synergistic behavior seems to be used by the Central Nervous System to generate coordinated movements, simultaneously activating different Degrees of Freedom (DoFs), instead of acting separately on each joint or muscle. The existence of these patterns was observed in different motor tasks and at different levels of the motor control architecture, i.e. neural [66], muscular [21, 65], kinematic [57, 43, 35]. For a review on these topics see e.g. [56]. Considering the kinematic level, such observations supported the idea that few combinations of the hand DoFs, e.g. described in terms of main principal components (PCs, i.e. postural synergies) of hand joint angles recorded e.g in grasping tasks, can take into account large part of hand pose variability. Higher order PCs are likely involved to describe more complex actions such as haptic exploration [67] and contact forces distribution [3].

Several statistical methods have been used to describe kinematics synergies, e.g. Principal Components Analysis (PCA), Single Value Decomposition (SVD), Functional PCA (fPCA) and Non-Negative Matrix Factorization (NNMF). In [57], PCA, applied to a dataset of grasping poses revealed that the first three PCs accounted for $\sim 90\%$ of the total hand poses variability, while the first two PCs accounted for $\sim 84\%$. These findings were then confirmed in other studies that take into account real object grasps [43] and the inter-digit coordination occurring during the whole grasping procedure.

While a lot of attention has been devoted to analyze hand behavior, little has been done to investigate synergistic control of the whole upper limb. In this chapter, we aim at bridging this gap moving from hand synergies to upper limb kinematics investigation, with the goal of unveiling the principal synergistic actuation pattern that underpin motion generation in space and time. At the same time, the avenue of soft, adaptable yet robust artificial grippers that can deform in a human-like manner to mold around different items and fully exploit environment to multiply

their degrees of freedom, has motivated our scientific interest in understanding the role of environmental constraints in synergistic control of human hands. This chapter is organized around these two topics, and their implications for the design and control of robotic devices.

2 Experimental setup for data acquisition

The correct investigation of main upper limb modes and the synergistic behavior of the human hand in interaction with the environment necessarily needs to move from accurate kinematic recordings. To achieve this goal, we employed a commercial system for 3D motion tracking with active markers (*Phase Space*®). Ten stereo-cameras working at 480Hz tracked 3D position of markers, which were rigidly attached to upper limb and hand links. We used 20 markers for upper limb acquisitions and additional 20 markers for hand kinematics tracking, four for each finger. We suitably designed and printed in ABS (see fig. 1a)rigid supports to accomodate markers. Data acquisition phase was implemented through a custom application developed in C++, using Boost libraries [60] to synchronize Phase Space recordings - obtained through OWL library data and force/torque sensors. The complete experimental setup is reported in figure 1.

In addition, we used two cameras (Logitech hd 1080p) to record the experiments scene to visually compare the real and reconstructed movement. Subjects wore Thimblesenses in all fingertips, which are wearable sensors that enable complete individual digit force/torque measurements and contact point estimation [7]. Since Thimblesense are composed by an external rigid shell worn at the fingertip level, their usage also provides cutaneous impairment. The latter aspect is very interesting to be investigated since it could provide useful guidelines for sensing soft robotic hands, as discussed later. during the tactile impairment experiments, as in Fig. 1e. Each shell is connected to the corresponding fingertip as in classical thimbles. Please refer to [7] for a more extensive description of the impairment effects of the shells. Force information acquired by these sensors was also aquired to be used in future investigations. Force/torque information was also measured on the object/environment side. To this purpose, a sensorized platform (600×400 mm), which includesforce-torque sensor ATI mini45E mounted as in Fig. 1f, was used to sense the interaction forces/torques with the table where objects were placed.

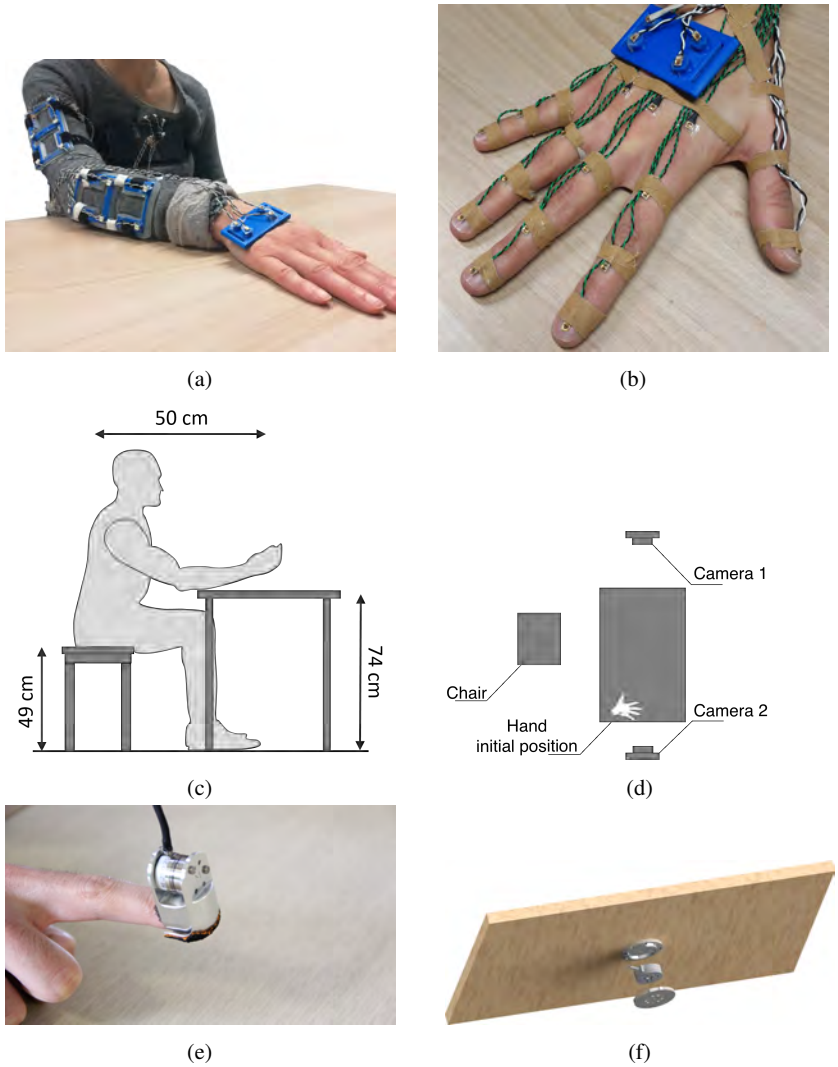

Fig. 1: In these figures we show the experimental setup. In a) and b) we report the markers accomodation for upper limb and hand, respectively. In c) and d) we show a schematic representation of the experimental setup. Subjects were comfortably seated in front of the table. In the starting position, the subject hand was located at the right side of the table. Two cameras are included to record the scene. In e) we show the shells at fingertip level, which produce tactile impairment and in f) an exploded view of the sensorized table.

3 Modeling

3.1 Modeling of upper limb kinematics

An accurate description of human upper limb is challenging due to the high complexity of the kinematic structure, e.g. for axis location and direction. To explore the system complexity, the interested reader can refer to [44, 37]. In this work, we used a trade-off between complexity and accuracy. This allows to get an acceptable computational time, still maintaining a good level of explanation of physical behaviour. Taking inspiration from [8], we adopted a model with 7 degrees of freedom (DoFs), and 3 invariable shape links. Joints angles are defined as $q_1, \ldots, q_7$: q_1 is associated to the shoulder abduction-adduction; q_2 is associated to the shoulder flexion-extension; q_3 is associated to the shoulder external-internal rotation; q_4 is associated to the elbow flexion-extension; q_5 is associated to the elbow pronation-supination; q_6 is associated to the wrist abduction-adduction; q_7 is associated to the wrist flexion-extension. In figure 2 a scheme of the model is reported.

To describe the forward kinematics of the arm, 5 different reference systems was defined: S_{ref}, centered in O_{ref}, fixed to the epigastrium; S_S, centered in O_S, Center of Rotation (CoR) of shoulder joints, fixed to the arm; S_E, centered in O_E, CoR of elbow joints, fixed to the forearm; S_W, centered in O_W, CoR of wrist joints, fixed to the hand; S_H, centered in O_H, fixed to the hand. The rigid transform between S_{ref}

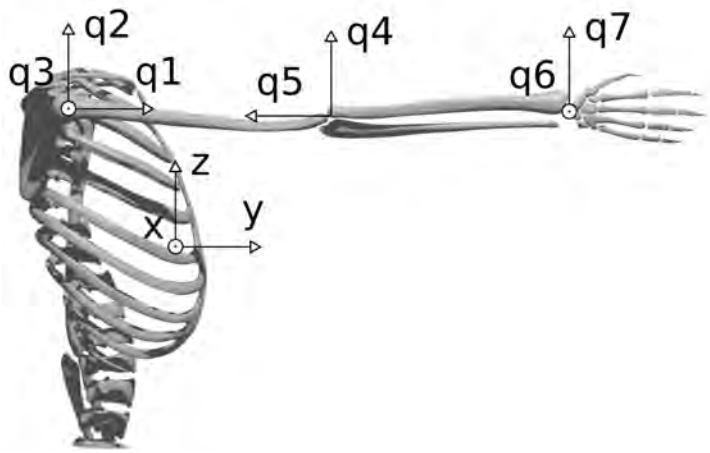

Fig. 2: Kinematic model of the upper limb.

and S_S is $T_{O_{ref}O_S}$; the rigid transform between S_S and S_E is $T_{O_SO_E}$; the rigid transform between S_E and S_W is $T_{O_EO_W}$; the rigid transform between S_W and S_H is $T_{O_WO_H}$.

To parameterize the *i-th* segment we use the *Product of Exponentials* (POE) formula [14]:

$$g_{O_{ref}O_j}(\theta) = \left[\prod_{k=1}^{j} e^{\hat{\xi}_k \theta_k}\right] g_{O_{ref}O_j}(0)$$

where $\hat{\xi}_k$ are the twists of the joints defining the kinematic chain,

$\theta = [\theta_1, \ldots, \theta_k, \ldots, \theta_j]^T$ are the exponential coordinates of the 2^{nd} kind for a local representation of SE(3) (Special Euclidean group, 4 x 4 rototranslation matrices) for the j-th link, and $g_{O_{ref}O_j}(0)$ is the initial configuration. For further details, the interested reader can refer to [33].

Links movements were tracked by fastening optical active markers to upper limb links through the rigid supports descrbed in the previous section. Markers positioning is inspired by [12]. In order to improve tracking performance, a redundant configuration of marker was used, in particular 4 markers fixed to the chest, 6 markers fixed to the lateral arm, 6 markers fixed to the dorsal forearm, 4 markers fixed to the hand dorsum. A picture showing marker distribution is reported in figure 1a. The position of each marker can be calculated as rigid transform with respect to (w.r.t.) the center of the corresponding support, while the support kinematic can be described as a rigid transform from the link reference system to the support reference system.

The model is completely parameterized using 14 parameters (calibrated for each subject as described later) collected in a vector p_G: Bones length (arm and forearm, 2 parameters); rigid transform from epigastrium to the shoulder CoR (3 parameters); rigid transform from shoulder CoR to the center of arm marker support (3 parameters); rigid transform from elbow CoR to the center of forearm marker support (3 parameters); rigid transform from wrist CoR to the center of hand marker support (3 parameters). The parameter vector p_G was calibrated for each subject. Given p_G, the upper limb pose is described by 7 joints angles $[q_1, \ldots, q_7]^T$ collected in a vector x.

3.2 Kinematic Model of the Human Hand

If the kinematic description of human upper limb is challenging, an accurate representation of human hand kinematics is even more challenging, due to the complex inter-play between different elements such as ligaments, muscles and joints. Fol-

lowing Occam's razor approach, we opted also in this case for a trade-off between accuracy and complexity, proposing a 20 DoF kinematic model (Fig. 3a). Each long finger is described by a set of four angles: two DoFs for flexion-extension and abduction-adduction in metacarpophalangeal joints, one DoF for flexion-extension in proximal and distal intra-phalangeal joints. The thumb is described with four angles: two DoFs for the trapeziometacarpal joint, one DoF for the metacarpo-phalangeal joint, and one DoF for the interphalangeal joint. For the sake of space, we do not report here the mathematical form of the kinematics , which can be easily derived from the Denavit-Hartenberg parametrization in Fig. 3b (see e.g. [45]). A key characteristic of the model is that it shares the 15 DoFs of the model used in [57], allowing an easy comparison with the classical postural synergy of grasp, as done e.g. in [33].

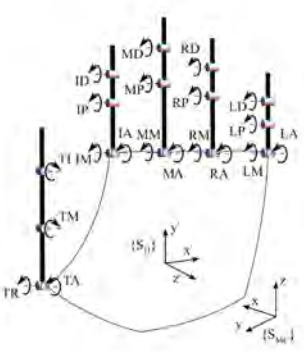

DoFs	Description
TA	Thumb Abduction
TR	Thumb Rotation
TM	Thumb Metacarpal
TI	Thumb Interphalangeal
IA	Index Abduction
IM	Index Metacarpal
IP	Index Proximal
ID	Index Distal
MM	Middle Metacarpal
MA	Middle Abduction
MP	Middle Proximal
MD	Middle Distal
RA	Ring Abduction
RM	Ring Metacarpal
RP	Ring Proximal
RD	Ring Distal
LA	Little Abduction
LM	Little Metacarpal
LP	Little Proximal
LD	Little Distal

(a) Kinematic model

Thumb (4 axis, 4R)

j	θ	d	a	α	offset
1	q_1	0	0	$-\frac{\pi}{2}$	0
2	q_2	0	a_2	$-\frac{\pi}{2}$	0
3	q_3	0	a_3	0	0
4	q_4	0	a_4	0	0

Long Finger (4 axis, 4R)

j	θ	d	a	α	offset
1	q_1	0	0	$-\frac{\pi}{2}$	0
2	q_2	0	a_2	0	0
3	q_3	0	a_3	0	0
4	q_4	0	a_4	0	0

(b) DH parametrization

Fig. 3: Kinematic model of the human hand considered in this work. The model has 20 DoFs, which include the 15 DoFs of the hand model used in [57]. The left panel graphically describes hand kinematics, while the right one specifies the Denavit-Hartenberg parametrization of thumb and the long fingers. We denoted with j the joint index, starting from the proximal joint to the distal, while q_1, q_2, q_3, q_4 are the joint angles, and a_2, a_3, a_4 are the phalanx lengths.

4 Motion Identification

The movement reconstruction - for both the upper limb and the hand movements - is based on a two-phase procedure: in a first step, we calibrated the model to retrieve an accurate estimation of the parameters (i.e. bones dimensions), then, we used this estimation as model for the joint angle estimation procedure based on an Extended Kalman Filter (EKF), which we applied at each time frame. In particular, the calibration procedure was implemented by solving a constrained least-squares minimization problem:

$$(x^*, p_G^*) = arg \min_{x_k \in D_x, p_G \in D_p} \frac{1}{2} \sum_{k=1}^{N_p} r_k^T r_k$$

The residual function r_k is calculated as $r_k(x_k, p_G) := y_k - f(x_k, p_G)$, where: y_k is the marker position vector measured with PhaseSpace; x_k is the vector of estimated joint angles; p_G is the vector of model kinematic parameters; D_x is the upper limb joint range of motion; D_p is the variation around a preliminary estimation of parameters performed with manual measurements; $f(x_k, p_G)$ is the estimated position vector of markers using the forward kinematics.

Taking inspiration from [33], the calibrated model was then used to identify the joints angles using an Extended Kalman Filter (EKF). Indeed, the model can be considered as an uncertain noisy process, where at the time frame k the joint angle vector x_k is the state of the process, y_k is the marker position vector, w_k and v_k are process and observation zero mean gaussian noises, with covariance Q_k and R_k, respectively, and $f(x_k)$ is the forward kinematics. The system can be described using the following equations:

$$\begin{cases} x_k = x_{k-1} + w_k \\ y_k = f(x_k) + v_k \end{cases} \tag{1}$$

Given the state at time frame $k-1$, the state at time k was obtained using a 2-steps procedure: *prediction* of the future state $\hat{x}_{k|k-1} = \hat{x}_{k-1}$; *update* of the state estimated in the first step by calculating $\hat{x}_{k|k} = \hat{x}_{k|k-1} + K_k \tilde{r}_k$. The correction amount of the state prediction is the product between the residual values vector $\tilde{r}_k = y_k - f(\hat{x}_{k|k-1})$ and the Kalman Gain K_k. This gain is calculated as product between the covariance matrix estimation of the predicted state $P_{k|k-1}$, the jacobian matrix, i.e. $H_k = \frac{\partial(f(x))}{\partial(x)}$, and the inverse matrix of the residual covariance. Both the covariance matrices are heuristically tuned.

The implementation described in this section was used for both the upper limb and hand movement reconstruction. Notwithstanding, the experiments that involved hand recordings was affected by an higher frequency of marker occlusions compared with the rest of the upper limb. This may cause degradation in reconstruction quality (more details in next sections). To face this problem, we introduced constrains in the identification procedure and developed an on-line adaptation of the observation noise covariance matrix by adding a scaling factor proportional to the number of consecutive missing measures (roughly speaking, the higher is the number of missing frames for the specific marker, the higher is the related observation noise covariance for the EKF)

5 Principal Functions for Upper Limb Movement Generation

5.1 Experiments

To develop a comprehensive study of human upper limb movements, one of the key features for the generation of a valid dataset is the definition of meaningful experimental actions[57, 43, 64, 69], which should ideally span all the range of motions under specific conditions. For this reason, we selected a set of movements driven by the study of grasping taxonomies [20, 30], and the analysis of human upper limb movement workspace [1, 48, 41]. The output of this selection resulted in a set of 30 different actions. In neuroscience, these movements can be classified in three classes, according to the presence or absence of an object and, if the object is present, on the approach with it: intransitive class, which collects actions that does not need the use of an object; transitive class, which collects actions that introduces the use of an object; tool mediated class, which collects actions where an object is used to interact with another one. The complete list of actions can be found in [5].

Seven adult right-handed subjects (5 male and 2 female, aged between 20 and 30), performed the experiment. Each task was repeated three times in order to increase the robustness of collected data. The experimenter gave the starting signal to subjects. In the instructions, the experimenter emphasized that the whole movement should be performed in a natural fashion. The object order was randomized for every subject. Each subject performed the whole experiment in a single day.

The performance of the estimation tool at each time frame k was evaluated by calculating the Mean Squared Error (MSE) R_k as

$$R_k = \frac{1}{N_{markers}} ||(y_k - f(\hat{x}_{k|k}))||$$

where $N_{markers}$ is the number of markers, y_k is the marker position vector and $f(\hat{x}_{k|k})$ is the vector of marker estimated positions using joint angles calculated with the EKF. Typical values of R_k are $\approx$ 1cm, with a mean error for hand and forearm markers of ≈ 0.5 cm and a mean error for arm markers of ≈ 1.8 cm.

5.2 Data Analysis

The goal of this work is the study of functional motor synergies of upper limb in space and time. More specifically, we are interested in identifying the underpinning functions that generate joint angle trajectories over time. This is accomplished using functional PCA, a statistical method that allows to study the differences in shapes between functions [52, 51]. In order to avoid the inclusion in this analysis of undesired features due to misalignments in time or in velocity of the samples, we implemented the following pre-processing techniques: (i) segmentation, to isolate each repetition for each task, (ii) time warping, to synchronize in time all the elements of the dataset.

1. **Segmentation**: it was used to segmentate the three repetitions of each action. The segmentation procedure selects the transition frame between repetitions as mean frame among two peaks. The mean value is weighted by the mean slopes of the curve before and after the transition frame.
2. **Time Warping**: it was used to make comparable in time different samples. Given two time series, v_1 and v_2, the affinity between the two signals is increased by the solution of the following least-squares minimization problem:

$$(S,T) = arg \min_{S>0,T} (||v_1(t) - v_2(St - T)||)$$

where S is a scaling factor for the velocity of signal v_2, and T is the amount of shifting in time applied to v_2. In this work, we warped all the signals w.r.t. the same reference to get a dataset of same-length vectors. The reference signal was selected as the element whose length is the mean value w.r.t. the length of all dataset elements.

5.2.1 Functional Principal Component Analysis

Functional PCA can be described as a functional extension of PCA. The first functional principal component $\xi_1(t)$ is the function for which the principal component score $f_{i1} = \int \xi_1(t)x_i(t)dt$ maximizes $\sum_i f_{i1}^2$ subject to $\int \xi_1^2(t)dt = ||\xi_1|| = 1$; the second functional principal component $\xi_2(t)$ maximizes $\sum_i f_{i2}^2$ subject to $||\xi_2|| = 1$ and $\int \xi_2(t)\xi_1(t)dt = 0$, and so on. In practice, this is done implementing the following steps:

1. Given a dataset of functions x_i and extract the mean signal $\bar{x}$ as $\bar{x_j} = \frac{1}{N}\sum_{i=1}^{N} x_{ij}$;
2. Remove the mean calculated in step 1 from each data element by $\tilde{x_i} = x_i - \bar{x}$;
3. Define a basis function. The basis must contain a number of functions large enough to consider all possible modes of variations of data. Usually basis elements can exponential functions, splines, Fourier basis [52, 50, 51];
4. Given the basis functions $b_1, \ldots, b_N$, each data element can be described as combination of basis elements $\tilde{x_i} = \sum_{k=1}^{N} \theta_k b_k$;
5. Then each function is described by a vector of coefficients $\Theta = (\theta_1, \ldots, \theta_N)'$;
6. PCA is now performed on these vectors. This leads to define the PCs, which are vectors of coefficients;
7. Each PC is, then, transformed into the corresponding function Principal Components (fPCs) using basis elements as $x_{rec} = \bar{x} + c_1\xi_1 + c_2\xi_2 + c_3\xi_3 + \ldots$;
8. Each fPC explains a certain percentage of variance. The variance explained by a fPC is quantified normalizing (w.r.t. the sum of the eigenvalues) the corresponding eigenvalue of the covariation matrix.

5.3 Results

We used fPCA on this dataset after the post-processing phase reported in previous sections. 15 5^{th} order spline basis elements were used, taking inspiration from the polynomial description in [31]. Each basis function is defined by piecewise polynomial functions. The places where the pieces of the spline intersect are known as knots. Each piece has the following form

$$s_k(t) = \sum_{i=1}^{5} a_{ik}(t - t_k)^i$$

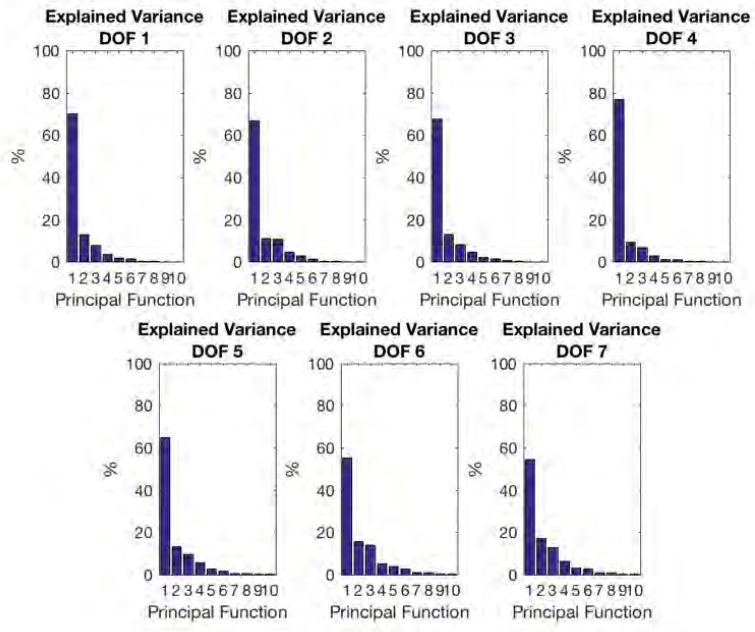

Fig. 4: Explained percentage variance for different DoFs and for each fPC. Each subplot refers to the correspondent joint of figure 2 (i.e. DoF1 refers to q1, and so on)

where t_k is the k^{th} knot. The fPCs can be used to reconstruct the data sample by adding M fPCs weighted by coefficients c_i, i.e. $x_{rec} = \bar{x} + c_1\xi_1 + \cdots + c_i\xi_i + \cdots + c_M\xi_M$ with $M \leq N$. The number of fPCs in use represents the level of truncation of the basis and hence the level of approximation in reconstructing joint angle profile in time.

The outcomes of this analysis reveal that the first fPC by itself accounts for 60-70% of the variation of joint angle profile w.r.t. the mean function, as reported in figure 4. What is also noticeable is that the reconstruction attained with the first fPCs provides good results, in fact the explained variance of the first three fPCs is higher than 84% for all DoFs. In figure 5 we show how the main principal functions can shape the reconstruction of individual joint trajectories. Individual basis function do not need to represent meaningful movements. What we would like to point out is that a combination of basis elements (plus an offset) could reproduce any original trajectory of the joint dataset. The reconstruction performance is shown in figure 6a, where an exemplary reconstruction using 1, 2 and 3 fPCs, respectively, is reported. In order to quantify the reconstruction performance, an index of reconstruction error can be evaluated as

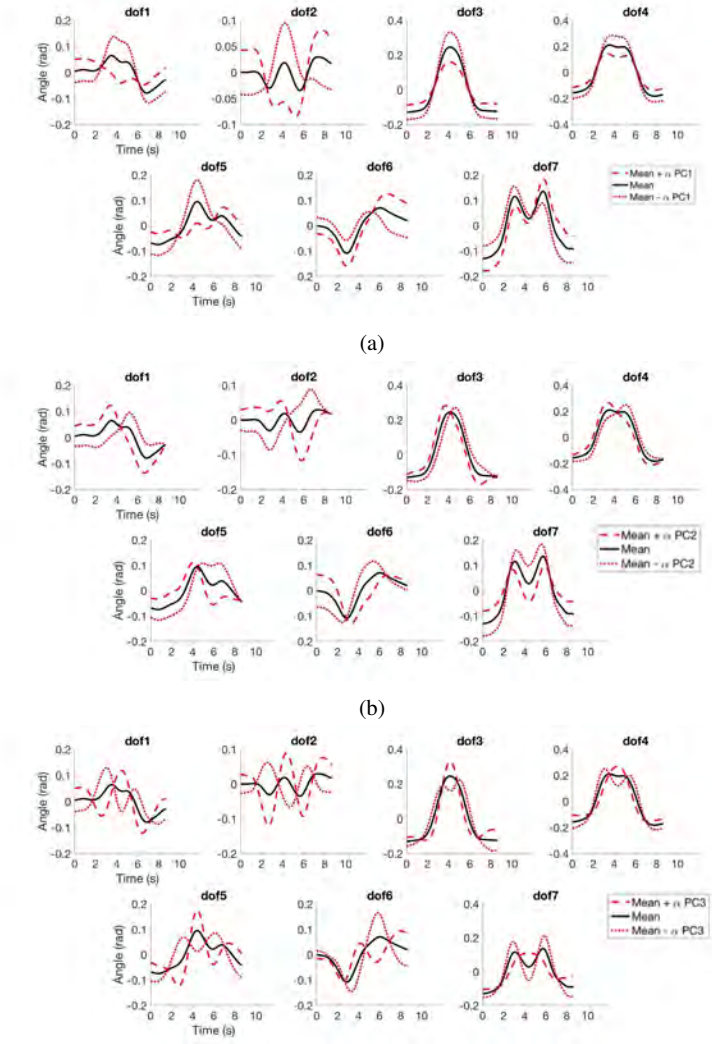

(a)

(b)

(c)

Fig. 5: In the top figure we report the mean function (in black) and the same mean function with the contribution of the first principal function, weighted with a coefficient α equal to one (with positive sign in red dashed line, with negative sign in red dotted line); in the central figure, we report the mean function (in black) and the same mean function with the contribution of the second principal function with a coefficient α equal to one (same legend of top figure); in the bottom figure we report the mean function (in black) and the same mean function with the contribution of the third principal function with a coefficient α equal to one (same legend of top figure)

$$E_{RMS} = \sqrt{\frac{1}{N_{DoF}} \sum_{i=1}^{N_{DoF}} (\sqrt{\frac{1}{N_{frames}} \sum_{j=1}^{N_{frames}} (x - x_{rec})^2})^2}$$

where x is the real function and x_{rec} is the reconstructed function.

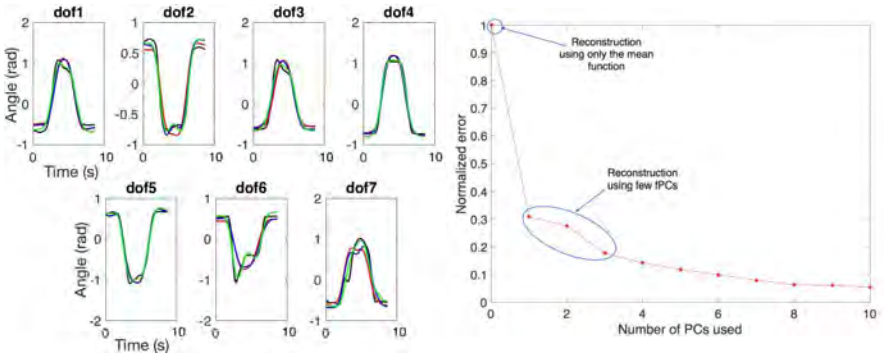

(a) Trajectories reconstruction. (b) Normalized Reconstruction Error (RMS).

Fig. 6: In the left figure. The black line represents the real data. The red line is the reconstructed data using the mean values and the first principal component. The blue line is the reconstructed data using the mean values and the first two principal components. The green line is the reconstructed data using the mean values and the first three principal components. In the right figure. The initial point refers to the error when only the mean function is used for reconstruction. The other points refers to the error when one or more fPCs are used for the reconstruction.

In figure 6b we plot the normalized error, calculated as $E_{RMS}/max(E_{RMS})$, for different numbers of fPCs in use. Initial point refers to the case where only mean function is used for reconstruction and the value of E_{RMS} is 0.6 *rad*. The reconstruction using one fPC has an E_{RMS} value lower than 0.2 *rad*, adding other fPCs, the reconstruction error decreases, i.e. using three fPCs the E_{RMS} value is around 0.1 *rad*. Furthermore, the whole reconstructed movement for the upper limb (considering all DoFs) was displayed using a visualization tool developed in MATLAB, showing an high level of anthropomorphism and realism. We can conclude that the kinematic complexity of upper limb trajectories can be simplified and easily described using the mean function and few principal functional modes for each joint.

6 Postural Hand Synergies during Environmental Constraint Exploitation

6.1 Experiments

In this section, we investigate the presence of a synergistic behavior underlying the generation of hand postures during the exploitation of environment, hereinafter referred to as Environmental Constraint Exploitation (ECE), execution and planning [22]. We also investigate the effect that cutaneous impairment might have on such synergies. We performed experiments with six participants (three females, three males; age range: $23-27$ years, mean 25.17 years), who were asked to grasp a set of objects from a flat surface. We selected this task since it represents a good trade-off between analytic complexity and richness of kinematic behavior induced by ECE [29]. For each trial, subjects were asked to reach the object posed in the center of the sensorized surface. Once the hand reached the object, subjects were asked to grasp, lift ($\sim$ 20 cm height), hold ($\sim$ 1 s), put it back on the table, and place the hand back to its starting position. Two trials were performed for any of the 21 objects. The object order was randomized for every subject. Two experimental conditions were considered: with and without cutaneous impairment. In the first case, participants were requested to wear rigid shells at their fingertips. Results were processed through Principal Component Analysis, as it is common in literature [55], in order to check the existence of a set of Principal Components describing the recorded data. We performed the analysis during the actual contact with the environment and on pre-shaping postures, i.e., during the approaching movement that precedes the hand-object-table interaction. Raw data collected from the experimental set-up were force and torque from the six axes F/T sensor ATImini45 of the sensorized platform, and 24 marker positions from the motion capture system, both with and without tactile impairment.

6.2 Data Pre-Processing and Analysis

Data processing is organized in two phases. First, data is pre-processed to reduce the noise and to evaluate joint angles and contact points. Second, we perform statistical analyses to identify the presence of a synergistic behavior in ECE. We perform the

analyses in pre-shaping, and during the whole contact with the environment. To quantify the role of tactile impairment, we consider separately the impaired and unimpaired cases.

The force/torque data from ATI Mini45 (i.e. sensorized surface) are filtered through a moving average filter based on Savitzky-Golay method [59]. The window width was heuristically tuned as the 1.5% of total data length. We then use the knowledge of surface form, to evaluate the centroid of contact of Force/Torque data and for contact-triggering.

We segment pre-processed data into three main phases, also described in Fig. 7: i) pre-shaping, where the object is reached and the hand posture is shaped in order to purposefully interact with the environment, ii) contact, in which the constraint is exploited in order to manipulate and grasp the object, and iii) post-contact, when the object is grasped and lifted from the table.

By considering non-adhesive interactions with the environment, we can assume any change occurring to the force orthogonal to the surface as due to an interaction. We thus segmented the actions searching for a change in the corresponding force measured by the sensorized surface. The cut off from the first and the second phase is identified by the first contact with the table, when the force starts to increase. To accurately detect this point we consider both the signal and its derivative. The cut off identifying the end of the contact phase is taken as the first time in which the contact force returns to zero.

The aim of the analysis is to identify a subspace of reduced dimensionality embedding the hand postures, to test the hypothesis of synergistic behavior in Environmental Constraint Exploitation. Principal Component Analysis (PCA) is a valuable tool to achieve this goal [57, 43, 63, 55]. Given a set of data, described by a correlation matrix C and a mean m, PCA derives an orthonormal base of the data space, whose first element S_1 indicates the direction where data present the greatest variability. In turn, each successive component S_i has the highest variability under orthogonality constraint. The $i-$th element of the base is referred to as Principal Component of the dataset. The normalized percentage of the data variability projected on each Principal Component is called explained variance of the component.

We evaluate PCA as the singular value decomposition of the data correlation matrix C, i.e. by finding an orthonormal matrix Σ, which brings C in Jordan form through the similitude transformation $\Sigma^T C \Sigma$. In that case the Principal Components are the columns of the matrix $\Sigma = [S_1, ..., S_n]$, and the explained variances are the corresponding eigenvalues. For further details on PCA we refer the interested reader

(a) Pre-shaping

(b) During contact

(c) Post-contact

Fig. 7: Photo-sequences of experimental constraint exploitation. According to our contact based classification, (a) shows the *pre-shaping* phase, (b) shows the *during contact* phase, and (c) the *post-contact* phase.

to [38]. If PCA is used to analyze hand postures in joint space, explained variances can be used to understand if the hand acts along a reduced set of the configurations by looking if there are few principal directions that explain the major part of the data . If this is the case we refer to such principal directions as synergies.

It is worth noticing that the use of the same calibrated kinematic model for every subject enables a coherent description of the hand configuration space in $\mathbb{R}^{20}$ for all the experimental conditions. We consider cosine of the angle between synergy directions as the metric to compare results of the different analyses. We evaluate it as the absolute value of the normalized dot product between the synergy vectors.

We also compare synergies resulting from our analysis with those employed for the execution of grasping, as shown in [57]. The kinematic model in [57] takes into account a subset of the joints considered in this work (see Sec. 3.2). Thus the configuration space of grasping synergies is a sub-set of dimension 15 of the hand configuration space considered in this work. To compare vectors, we projected full hand configurations in the corresponding sub-space. This is equivalent to simply neglect the values corresponding to joints ID, MD, RD and LD in Fig. 3a, as also done in [33].

6.2.1 Pre-shaping analysis

The pre-shaping analysis is done with the purpose of identifying kinematic regularities in the generation of hand postures for the ECE exploitation. In [57] PCA is performed for constant postures acquired in grasping. There authors took out effects due to interaction with the objects, by asking subjects to grasp imagined ones. In this analysis we aim to achieve the same goal by performing PCA on a dataset composed of the last poses before the contact with the environment in each trial, i.e. the last pose in pre-shaping phases when a purposeful interaction with the environment is planned. Unimpaired and impaired cases are separately analyzed. Both datasets are composed of 252 poses (six subjects, 21 objects, two trials)

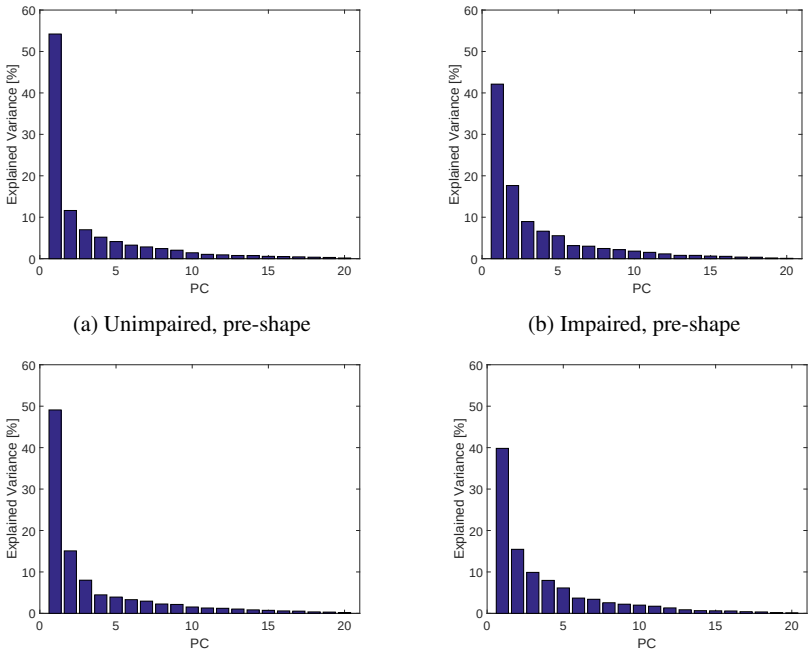

(a) Unimpaired, pre-shape

(b) Impaired, pre-shape

(c) Unimpaired, contact

(d) Impaired, contact

Fig. 8: Explained variance resulting from PCA analysis of postures in pre-shaping and during contact, in tactile impaired and unimpaired case. A marked predominance of the first Principal Component is present in all the cases, showing a synergistic behavior.

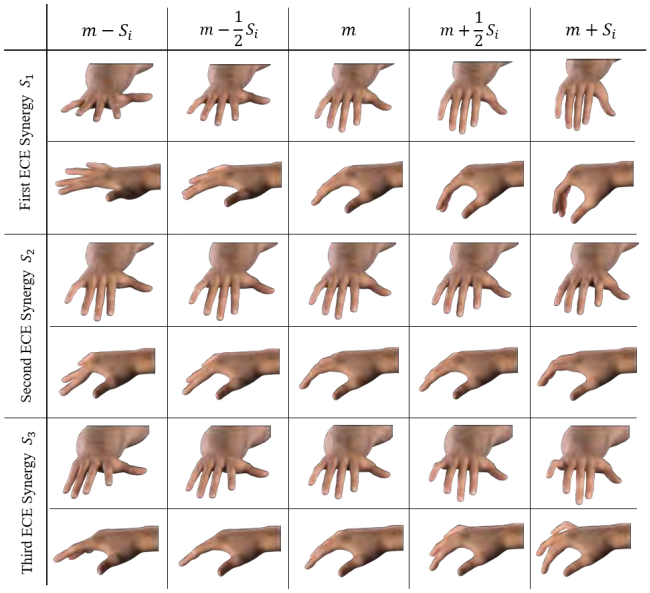

Fig. 9: Graphical representation of the hand shapes w.r.t. the mean posture, associated to the first three synergies during pre-shaping in unimpaired condition. Each column presents a different stage of the synergistic posture generation, obtained by summing the hand mean configuration m, to the synergy vector S_i of the $i-th$ synergy.

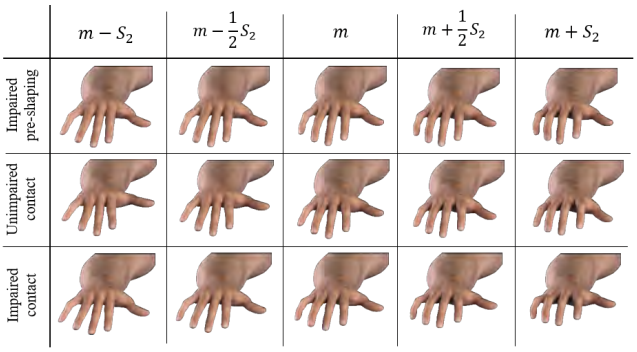

Fig. 10: Graphical representation of the hand shapes associated to the second ECE synergy. Pre-shaping impaired, contact unimpaired and contact impaired conditions are considered. The mean posture is referred as m, the second synergy as S_2. We do not report here the first synergy for each condition, since there are not significant and visible discrepancies. The figure also shows a good coherence in the behavior described by the second synergy, among the considered conditions.

6.2.2 Contact analysis

In order to evaluate if there are some kinematic regularities in the strategies employed by the subjects during actual exploitation of the surface, we perform PCA on data collected during the contact phase. We perform the analysis separately for the impaired and unimpaired case. To characterize the effect of cutaneous impairment we also evaluated the mean amount of time in which subjects remained in contact with the table, mean time for task accomplishment, and the mean norm of interaction forces, by averaging the corresponding values for every subject and every object.

The datasets for both impaired and unimpaired conditions are composed of a variable number of poses depending on the strategy execution time. Each ECE generates an amount of postures equal to 40 times the execution time (the acquisition rate is 40Hz). All 21 objects, two trials and six subjects were considered.

6.2.3 Differences between Pre and During contact

We investigate the persistence of the same basic ingredients of hand posture before and during the contact with the environment for both bare fingers and cutaneous impairment conditions. The dot product of synergies evaluated in previous sections was computed in order to quantify their similarities.

6.3 Results

6.3.1 Pre-shaping analysis

Fig. 8 shows the explained variance associated to the PCs on the poses during the pre-shaping phase. For the unimpaired case, the first Principal Component explains about 54% of the variance, while the first three pre-shaping synergies explain more than 72%. Fig. 9 shows the graphical representation of the first three resulting postural synergies. The same analysis in the impaired case shows that the first synergy explains about 42% of the variance, while three Principal Components explain more than 68% of the variance. Thus, for our dataset, the variance explained by the first main synergies is lower in the impaired condition. In Fig. 9 we present the graphical representations of the synergistic posture reconstruction corresponding to the first three synergies of pre-shaping without tactile impairment. Tab. 1 presents

the numerical values of the first ECE synergy of pre-shaping with and without impairment, in comparison with the first synergy of grasp [57]. Fig. 10 presents the movement corresponding to the second synergy of pre-shaping with tactile impairment.

In all the considered cases, the first synergy describes an opening-closing behavior of the whole hand, while the second synergy corresponds to a closure of the distal joints mostly of index and medial fingers, and a closing of the thumb. The third synergy is similar to the second, but concerning the little and ring fingers.

Fig. 11(a) shows the scalar product between the first grasp synergy in [57] and the ones found in this work for both sensory conditions. What is noticeable is that there is a high level of consistency between the main synergy of grasping and pre-shaping of human hand in impaired and unimpaired conditions (≥ 0.9). The similarity is reduced for the second synergy, as shown in the same Fig. (b), and so on for the other orders. Fig. 11 reports also a high correlation between pre-shaping synergies with

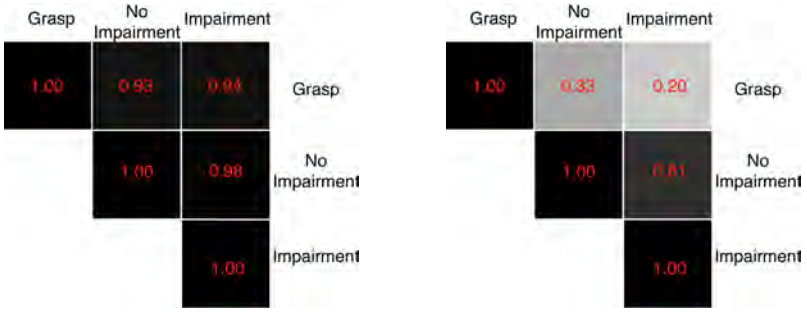

(a) First Synergies (b) Second Synergies

Fig. 11: Dot products between first and second grasp synergies and first and second ECE synergies evaluated during pre-shaping, with and without tactile impairment. The gray scale graphically codes the product value: black is 1, i.e. very similar, white is 0, i.e. very different. A high correlation between the first grasping and ECE synergies is evidenced. The ECE synergies with and without impairment present high similarity, which however drops for higher order synergies.

and without tactile impairment. The presence of impairment does not alter the first two synergies during the pre-shaping phase. However the similarity strongly drops when the synergy order increases further, reaching 0.36 for the third and 0.003 for the forth.

6.3.2 Contact analysis

In the unimpaired condition, the first Principal Component explains about the 49% of the variance, and the first three synergies more than 73%. The same analysis in the impaired case returns a first synergy explaining about the 39% of the variance, and the three Principal Components explaining more than 65% of the variance. Also in this case, for our dataset the percentage of variance explained in the impaired condition is lower. Tab. 1 presents the numerical values of first ECE synergy during the contact with the environment, with and without impairment, in comparison with the first synergy of grasp [57]. Fig. 10 presents the posture corresponding to the second synergy with and without tactile impairment.

Table 1: Numerical values of the first synergy of Grasp [57] and of Enviromental Constraint Exploitation, with and without impairment, before and after contact. We indicate with 'x' the DoFs that were not considered in [57].

DoFs	**Grasp**	**Unimpaired Pre-Shape**	**Impaired Pre-Shape**	**Unimpaired Contact**	**Impaired Contact**
TA	-0.43	-0.14	-0.15	-0.12	-0.15
TR	0.29	0.31	0.35	0.30	0.34
TM	0.14	0.14	0.17	0.17	0.16
TI	0.03	0.04	0.05	0.05	0.09
IA	-0.13	-0.08	-0.12	-0.08	-0.11
IM	0.33	0.39	0.35	0.40	0.34
IP	0.15	0.16	0.16	0.17	0.20
ID	x	0.01	0.03	0.03	0.05
MA	x	-0.03	-0.08	-0.02	-0.06
MM	0.33	0.38	0.33	0.38	0.32
MP	0.16	0.27	0.27	0.27	0.30
MD	x	0.04	0.06	0.05	0.08
RA	0.06	0.00	-0.02	0.02	-0.02
RM	0.40	0.44	0.37	0.43	0.32
RP	0.20	0.22	0.27	0.22	0.35
RD	x	0.04	0.06	0.05	0.11
LA	0.14	0.05	0.1	0.08	0.09
LM	0.37	0.43	0.42	0.41	0.37
LP	0.27	0.12	0.21	0.17	0.24
LD	x	0.02	0.04	0.02	0.08

The analysis also demonstrates that subjects with tactile impairment are in contact with the table for an average time of 4.2 ± 3.1s, while for the unimpaired case the

average time is 2.4 ± 2.4s. The complete task is performed in 13.9 ± 2.7s for the tactile impairment case, while it is performed in 11.5 ± 2.0s in the other case. Finally, the contact force is different for the experiments considered. Mean value of norm of contact forces for the tactile impairment case is 23.2 ± 8.6 N, while mean value is 12.3 ± 5.7 N in the other case.

6.3.3 Differences between Pre and During contact

The result shows that the first Principal Components in unimpaired and impaired conditions are very similar w.r.t. the corresponding ones of the pre-shaping analysis. The similarity tends to decrease with the increase of synergy order (correlation ≥ 0.75 till 9th synergy). Dot products are graphically reported in Fig. 12 for the unimpaired case. Thus ECs induce only changes for the high order synergies, leaving unaltered the main ones, regardless of availability of tactile input. Note that the first synergy is still equivalent to the one in [57].

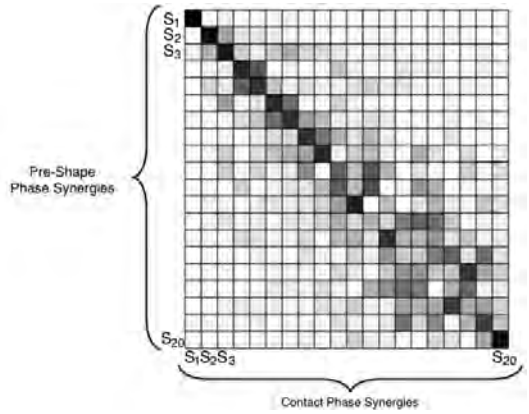

Fig. 12: Dot products between the ECE synergies in pre-shaping and in contact with the environment, in the bare finger case. The gray scale graphically codes the product value: black is 1, i.e. very similar, white is 0, i.e. very different. A tendency to maintain the first main components before and after the contact results clearly from this analysis. The results for the impaired case are analogous.

6.3.4 Inference and Statistical Relevance

In the previous sections we presented results from 6 subjects. Despite such a moderate number of participants, findings and analyses are in line with the existing literature in the field, see e.g. [57, 43, 47]. To generalize, we here report additional statistical analyses that provide t–Student based confidence intervals (CI) with 95% probability. CI refers to dot products performed on the PCs extracted for the different conditions, and the ones obtained in grasping.

CI for the dot product between the first synergy for impaired and unimpaired conditions is $[0.81, 0.96]$; CI for the dot product between the first grasping synergy and the unimpaired first ECE synergy is $[0.88, 0.94]$; CI for the dot product between the first grasping synergy and the impaired first ECE synergy is $[0.79, 0.9]$. Regarding the contact analysis of Sec. 6.3.3, the dot product between the first Principal Component before and during contact results in a CI of $[0.97, 0.99]$ (unimpaired case).

7 Implications for Robotics and Motor Control

In this chapter we have focused on characterizing the human upper limb and hand movements. In particular, the first problem has been faced through a functional approach, which showed that the complexity of upper limb movements in activities of daily living can be described using a reduced number of functional principal components. To achieve this goal we developed an experimental setup, which is based on kinematic recordings but also allows to include additional sensing modalities. Kinematic data are based on a 7 DoFs model and are quantified through a calibration-identification procedure. Collected data was used to characterize upper limb movements through functional analysis. The findings of this work can be used to pave the path towards a more accurate characterization of human upper limb principal modes, opening fascinating scenarios in rehabilitation, e.g. for automatic recognition of physiological and pathological movements.(e.g. stroke affected subjects) through machine learning.

At the same time, the here reported results and future investigations could also offer a valuable inspiration for the design and control of robotic manipulators. First, recognizing that few principal modes describe most of kinematic variability could provide insights for a more effective planning and control of robotic manipulators.

For the planning phase, using input trajectories as combinations of the main functional components, which explain most of the kinematic variability in time, could represent a succesful initial guess to control the movement of the robot – eventually combined with a feedback correction. This combination of feedforward and feedback components could be successfully employed also with soft robotic manipulators, i.e. robots designed to embody safe and natural behaviors relying on compliant physical structures purposefully used to achieve desirable and sometimes variable impedance characteristics. In these cases, standard methods of robotic control can effectively fight against or even completely cancel the physical dynamics of the system, replacing them with a desired model - which defeats the purpose of introducing physical compliance. To overcome this limitation in [23] an anticipative model of human motor control was proposed, which used a feedforward action combined with low-gain feedback, with the goal of obtaining human-like behavior through iterative learning. Results presented in this work could be used to define the feedforward component for the control of soft robots. Second, using human-like primitives for controlling robotic systems could improve the effectiveness and safety of Human - Robot Interaction (HRI). Indeed, several studies identified anthropomorphism as one of the key enabling factor for successful, acceptable, predictable and safe HRI in many fields, such as human robot co-working and rehabilitative/assistive robotics [6, 26, 27, 53].

Furthermore, the here reported experimental and analytical framework could be used to identify principal actuation schemes for under-actuated robotic devices. As an example, in [16], we used the identification procedure and the kinematic model reported in this work to estimate the contribution of wrist joints in the most common poses for grasping. We performed PCA on the estimated joints of the wrist pre-grasp poses and we found that the flexo-extension DoF plays a dominant role. We used these results to calibrate an under-actuated wrist system, which is also adaptable and allows to implement different under-actuation schemes, demonstrating its effectiveness to accomplish grasping and manipulation tasks.

Future works will aim at using functional data to allow a dynamic implementation of principal kinematic modes of human upper-limb in robotic systems. Finally, the integration of other sensing modalities, such as Electro-encephalographic recordings, could be used to study neural correlates of human upper limb motions, thus possibly inspiring the development of effective Brain-Machine Interfaces for assistive robotics.

Regarding the hand movements, we implemented a PCA-based analysis to achieve a synergistic description of hand control in case of Environmental Constraint Exploita-

tion, during pre-shaping and contact phase, and with or without tactile impairment. In particular, we showed that the explained variance reported in Fig. 8 suggests the presence of an underlying synergistic behavior in the purposeful exploitation of environmental constraints. Indeed, the space dimensionality required to approximate hand posture is considerably smaller than the number of degrees of freedom. In particular, the first Principal Component shows a marked predominance, with a maximum total variance explained of 54% in the unimpaired pre-shaping case. The three first synergies explain more than 65% of the total variance in all the conditions. In the experiments, during contact with the environment, the amount of variability accounted by higher order synergies increases. This could be explained by observing that the interaction can shape the subject hand beyond its nominal kinematics. This behavior is also in agreement with the findings in [58], where the synergistic analysis of [57] was performed on grasped real objects instead of imagined ones.

Despite our inference analysis (Sec. 6.3.4) is limited to the first synergy, a series of characteristics of our dataset can be pointed out, which are in accordance with existing neuroscientific findings. Future works will focus on different experimental procedures and tasks to further investigations. In our dataset, the first two synergies in the impaired and unimpaired conditions are very similar, as shown in Fig. 10 and Fig. 11. This suggests that the presence of tactile impairment, while modifying the strategies themselves, does not substantially modify the most basic kinematic ingredients commonly used to generate hand postures (for more details please refers also to [4]). Subjects are aware of the presence of the tactile impairment, so it is reasonable to expect that they might have changed their planning in accordance to that. Indeed, the drop of such similarity after the third synergy suggests that cutaneous impairment affects posture refinement, which can be likely ascribed to higher order synergies (as described in [57]). However the amount of data collected does not allow a sound statistical characterization of this behavior. To assess whether higher order synergies are primarily noise or they actually contribute to hand postures, we will resort to the usage of discriminant analysis and information theory, as in [57], as future works.

Analogously, Fig. 12 shows a high similarity in the first Principal Components during contact and pre-shaping, while differences can be observed for higher order synergies. Uncontrolled Manifold theory [61, 40] suggests that the central nervous system selects in the space of joint angles a subset of variables of interest, which are regulated, purposefully leaving free the remaining variables. The persistence of main postural synergies of pre-shaping during the contact with the environment can be

interpreted in the light of this theory by considering the first set of ECE synergies as the variables of interest for the considered task, which remain constant when an external disturbance occurs. The sub-space individuated by the higher order synergies is instead left free to adapt to the external environment. Moreover such behaviour could also be due to peripheral constraints embedded in the musculoskeletal system, as discussed e.g. in [55].

Data shown in Fig. 11 and Table 1 demonstrate that a strong resemblance exists between the first synergy, resulting from the analysis of ECE strategies, and the first synergy of grasp as found in [57]. This could suggest the presence of underlying synergies, which are integrated with task specific ones. This was proposed e.g. in [34], and it is in agreement with experimental results presented in [63], where task independent synergies are estimated by a set of unconstrained tasks (see CI estimates in section 6.3.4).

As it can be widely observed in literature, neuroscientific results of synergistic behavior of human hands have been successfully translated and applied to robotics to inform the design, control and sensing of artificial systems, with special focus on grasping, see [11, 10]. One of the first notable application of synergies to robotics was in [15], where authors propose to use grasp synergies to derive actuation patterns for an underactuated robotic hand. In [32], the use of hand synergies for the choice of grasping forces was discussed. In [19] and later in [2, 68, 42], a synergy based low-dimensional synergistic space is considered to obtain effective pre-grasp shapes for fully actuated robotic hands.

Recently, synergy-inspired actuation has been combined with the introduction of compliance in the structure [17, 70, 24, 25, 18] (according to the soft synergy framework [11]). The availability of robotic hands embedding elasticity in their mechanics has also led to a shift in their control philosophy, accounted e.g. in [13, 28]. In the classical planning, suitable points are selected on the object to be grasped or manipulated, generating a nominal grasp of good quality. Trajectories are then executed, to correctly position the fingertips while avoiding contacts with the environment. On the contrary, soft manipulation has changed this scheme. The hand-environment contacts are no more avoided but exploited to successfully shape the hand around the object. Under this regard, the study of environmental exploitation in humans could inform the design, planning, and control of robotic hands to take full advantage from the external environment.

The most direct implication of the presented results could leverage upon the observation that the first synergy of grasping is very similar to the first synergy for

Environmental Constraint Exploitation (ECE). Thus the implementation of the first synergy of grasp as degree of actuation can target the twofold goal of realizing under-actuated robotic hands that can effectively grasp objects and, at the same time, are able to exploit Environmental Constraints. To increase hand functionalities beyond the first degree of actuation, we could implement additional ECE synergies, possibly in combination with the grasp synergies. For some examples of the implementation of synergies for the design of under-actuated robotic hands, we refer the interested reader to [36, 24, 49].

Looking at the differences between the impaired and unimpaired conditions, the key kinematic ingredients seem to remain unaltered at least for the gross movements. However, the time for task accomplishment and the force exchanged with the environment is higher for the impaired case. This result could indicate possible sensing strategies for soft robotic hands, i.e. to detect contact with the environment e.g. through IMU sensors, which can lead to the development of planning and control laws aiming at minimizing force execution on external objects.

Acknowledgements This research has received funding from the European Union's Horizon 2020 Research and Innovation Programme under Grant Agreement No.688857 (SoftPro).

References

1. Abdel-Malek, K., Yang, J., Brand, R., Tanbour, E.: Towards understanding the workspace of human limbs. Ergonomics **47**(13), 1386–1405 (2004)
2. Amor, H.B., Kroemer, O., Hillenbrand, U., Neumann, G., Peters, J.: Generalization of human grasping for multi-fingered robot hands. In: Intelligent Robots and Systems (IROS), 2012 IEEE/RSJ International Conference on, pp. 2043–2050. IEEE (2012). DOI 10.1109/iros.2012.6386072
3. Averta, G., Angelini, F., Bonilla, M., Bianchi, M., Bicchi, A.: Incrementality and hierarchies in the enrollment of multiple synergies for grasp planning. IEEE Robotics and Automation Letters (2018)
4. Averta, G., Della Santina, C., Battaglia, E., Ciotti, S., Arapi, V., Fani, S., Bianchi, M.: From humans to robots: The role of cutaneous impairment in human environmental constraint exploitation to inform the design of robotic hands. In: Ultra Modern Telecommunications and Control Systems and Workshops (ICUMT), 2017 9th International Congress on, pp. 179–184. IEEE (2017)
5. Averta, G., Della Santina, C., Battaglia, E., Felici, F., Bianchi, M., Bicchi, A.: Unveiling the principal modes of human upper limb movements through functional analysis. Frontiers in Robotics and AI **4**, 37 (2017)

6. Bartneck, C., Kulić, D., Croft, E., Zoghbi, S.: Measurement instruments for the anthropomorphism, animacy, likeability, perceived intelligence, and perceived safety of robots. International journal of social robotics **1**(1), 71–81 (2009)
7. Battaglia, E., Bianchi, M., Altobelli, A., Grioli, G., Catalano, M.G., Serio, A., Santello, M., Bicchi, A.: Thimblesense: a fingertip-wearable tactile sensor for grasp analysis. IEEE transactions on haptics **9**(1), 121–133 (2016)
8. Benati, M., Gaglio, S., Morasso, P., Tagliasco, V., Zaccaria, R.: Anthropomorphic robotics. Biological Cybernetics **38**(3), 125–140 (1980)
9. Bernstein, N.A.: The control and regulation of movements (1967)
10. Bianchi, M., Moscatelli, A.: Human and Robot Hands: Sensorimotor Synergies to Bridge the Gap Between Neuroscience and Robotics. Springer (2016)
11. Bicchi, A., Gabiccini, M., Santello, M.: Modelling natural and artificial hands with synergies. Phil. Trans. R. Soc. B **366**(1581), 3153–3161 (2011). DOI 10.1098/rstb.2011.0152
12. Biryukova, E., Roby-Brami, A., Frolov, A., Mokhtari, M.: Kinematics of human arm reconstructed from spatial tracking system recordings. Journal of biomechanics **33**(8), 985–995 (2000)
13. Bonilla, M., Farnioli, E., Piazza, C., Catalano, M., Grioli, G., Garabini, M., Gabiccini, M., Bicchi, A.: Grasping with soft hands. In: Humanoid Robots (Humanoids), 2014 14th IEEE-RAS International Conference on, pp. 581–587. IEEE (2014). DOI 10.1109/HUMANOIDS.2014.7041421
14. Brockett, R.W.: Robotic manipulators and the product of exponentials formula. In: Mathematical theory of networks and systems, pp. 120–129. Springer (1984)
15. Brown, C.Y., Asada, H.H.: Inter-finger coordination and postural synergies in robot hands via mechanical implementation of principal components analysis. In: Intelligent Robots and Systems, 2007. IROS 2007. IEEE/RSJ International Conference on, pp. 2877–2882. IEEE (2007). DOI 10.1109/iros.2007.4399547
16. Casini, S., Tincani, V., Averta, G., Poggiani, M., Della Santina, C., Battaglia, E., Catalano, M.G., Bianchi, M., Grioli, G., Bicchi, A.: Design of an under-actuated wrist based on adaptive synergies. In: Robotics and Automation (ICRA), 2017 IEEE International Conference on, pp. 6679–6686. IEEE (2017)
17. Catalano, M.G., Grioli, G., Farnioli, E., Serio, A., Piazza, C., Bicchi, A.: Adaptive synergies for the design and control of the pisa/iit softhand. The International Journal of Robotics Research **33**(5), 768–782 (2014). DOI 10.1177/0278364913518998
18. Chen, W., Xiong, C.: On adaptive grasp with underactuated anthropomorphic hands. Journal of Bionic Engineering **13**(1), 59–72 (2016). DOI 10.1016/s1672-6529(14)60160-8
19. Ciocarlie, M., Goldfeder, C., Allen, P.: Dexterous grasping via eigengrasps: A low-dimensional approach to a high-complexity problem. In: Robotics: Science and Systems Manipulation Workshop-Sensing and Adapting to the Real World (2007)
20. Cutkosky, M.R.: On grasp choice, grasp models, and the design of hands for manufacturing tasks. IEEE Transactions on robotics and automation **5**(3), 269–279 (1989)
21. d'Avella, A., Saltiel, P., Bizzi, E.: Combinations of muscle synergies in the construction of a natural motor behavior. Nature neuroscience **6**(3), 300 (2003)

22. Della Santina, C., Bianchi, M., Averta, G., Ciotti, S., Arapi, V., Fani, S., Battaglia, E., Catalano, M.G., Santello, M., Bicchi, A.: Postural hand synergies during environmental constraint exploitation. Frontiers in neurorobotics **11**, 41 (2017)
23. Della Santina, C., Bianchi, M., Grioli, G., Angelini, F., Catalano, M., Garabini, M., Bicchi, A.: Controlling soft robots: balancing feedback and feedforward elements. IEEE Robotics & Automation Magazine **24**(3), 75–83 (2017)
24. Della Santina, C., Grioli, G., Catalano, M., Brando, A., Bicchi, A.: Dexterity augmentation on a synergistic hand: the pisa/iit softhand+. In: Humanoid Robots (Humanoids), 2015 IEEE-RAS 15th International Conference on, pp. 497–503. IEEE (2015). DOI 10.1109/humanoids.2015.7363595
25. Della Santina, C., Piazza, C., Grioli, G., Catalano, M., Bicchi, A.: Towards dexterous manipulation with augmented adaptive synergies: the pisa/iit softhand 2. In: IEEE transactions on Robotics, in press. IEEE (2018)
26. Dragan, A., Srinivasa, S.: Integrating human observer inferences into robot motion planning. Autonomous Robots **37**(4), 351–368 (2014)
27. Duffy, B.R.: Anthropomorphism and the social robot. Robotics and autonomous systems **42**(3), 177–190 (2003)
28. Eppner, C., Brock, O.: Planning grasp strategies that exploit environmental constraints. In: Robotics and Automation (ICRA), 2015 IEEE International Conference on, pp. 4947–4952. IEEE (2015). DOI 10.1109/icra.2015.7139886
29. Eppner, C., Deimel, R., Álvarez-Ruiz, J., Maertens, M., Brock, O.: Exploitation of environmental constraints in human and robotic grasping. The International Journal of Robotics Research p. 0278364914559753 (2015). DOI 10.1007/978-3-319-28872-7_23
30. Feix, T., Romero, J., Schmiedmayer, H.B., Dollar, A.M., Kragic, D.: The grasp taxonomy of human grasp types. IEEE Transactions on Human-Machine Systems **46**(1), 66–77 (2016)
31. Flash, T., Hogan, N.: The coordination of arm movements: an experimentally confirmed mathematical model. The journal of Neuroscience **5**(7), 1688–1703 (1985)
32. Gabiccini, M., Bicchi, A., Prattichizzo, D., Malvezzi, M.: On the role of hand synergies in the optimal choice of grasping forces. Autonomous Robots **31**(2-3), 235–252 (2011)
33. Gabiccini, M., Stillfried, G., Marino, H., Bianchi, M.: A data-driven kinematic model of the human hand with soft-tissue artifact compensation mechanism for grasp synergy analysis. In: 2013 IEEE/RSJ International Conference on Intelligent Robots and Systems, pp. 3738–3745. IEEE (2013)
34. Gorniak, S.L., Zatsiorsky, V.M., Latash, M.L.: Hierarchies of synergies: an example of two-hand, multi-finger tasks. Experimental brain research **179**(2), 167–180 (2007). DOI 10.1007/s00221-006-0777-z
35. Grinyagin, I.V., Biryukova, E.V., Maier, M.A.: Kinematic and dynamic synergies of human precision-grip movements. Journal of neurophysiology **94**(4), 2284–2294 (2005)
36. Grioli, G., Catalano, M., Silvestro, E., Tono, S., Bicchi, A.: Adaptive synergies: an approach to the design of under-actuated robotic hands. In: Intelligent Robots and Systems (IROS), 2012 IEEE/RSJ International Conference on, pp. 1251–1256. IEEE (2012). DOI 10.1109/iros.2012.6385881

37. Holzbaur, K.R., Murray, W.M., Delp, S.L.: A model of the upper extremity for simulating musculoskeletal surgery and analyzing neuromuscular control. Annals of biomedical engineering **33**(6), 829–840 (2005)
38. Jolliffe, I.: Principal component analysis. Wiley Online Library (2002). DOI 10.1007/978-3-642-04898-2_455
39. Latash, M.L.: Synergy. Oxford University Press (2008)
40. Latash, M.L., Scholz, J.P., Schöner, G.: Toward a new theory of motor synergies. Motor control **11**(3), 276–308 (2007). DOI 10.1123/mcj.11.3.276
41. Lenarcic, J., Umek, A.: Simple model of human arm reachable workspace. IEEE transactions on systems, man, and cybernetics **24**(8), 1239–1246 (1994)
42. Malhotra, M., Rombokas, E., Theodorou, E., Todorov, E., Matsuoka, Y.: Reduced dimensionality control for the act hand. In: Robotics and Automation (ICRA), 2012 IEEE International Conference on, pp. 5117–5122. IEEE (2012). DOI 10.1109/icra.2012.6224651
43. Mason, C.R., Gomez, J.E., Ebner, T.J.: Hand synergies during reach-to-grasp. Journal of Neurophysiology **86**(6), 2896–2910 (2001)
44. Maurel, W., Thalmann, D.: Human shoulder modeling including scapulo-thoracic constraint and joint sinus cones. Computers & Graphics **24**(2), 203–218 (2000)
45. Murray, R.M., Li, Z., Sastry, S.S., Sastry, S.S.: A mathematical introduction to robotic manipulation. CRC press (1994)
46. Mussa-Ivaldi, F.A.: Modular features of motor control and learning. Current opinion in neurobiology **9**(6), 713–717 (1999). DOI 10.1016/s0959-4388(99)00029-x
47. Naceri, A., Santello, M., Moscatelli, A., Ernst, M.O.: Digit position and force synergies during unconstrained grasping. In: Human and Robot Hands, pp. 29–40. Springer (2016). DOI 10.1007/978-3-319-26706-7_3
48. Perry, J.C., Rosen, J., Burns, S.: Upper-limb powered exoskeleton design. IEEE/ASME transactions on mechatronics **12**(4), 408 (2007)
49. Piazza, C., Della Santina, C., Catalano, M., Grioli, G., Garabini, M., Bicchi, A.: Softhand pro-d: Matching dynamic content of natural user commands with hand embodiment for enhanced prosthesis control. In: Robotics and Automation (ICRA), 2016 IEEE International Conference on, pp. 3516–3523. IEEE (2016)
50. Ramsay, J.O.: Functional data analysis. Wiley Online Library (2006)
51. Ramsay, J.O., Hooker, G., Graves, S.: Functional data analysis with R and MATLAB. Springer Science & Business Media (2009)
52. Ramsay, J.O., Silverman, B.W.: Applied functional data analysis: methods and case studies, vol. 77. Citeseer (2002)
53. Riek, L.D., Rabinowitch, T.C., Chakrabarti, B., Robinson, P.: How anthropomorphism affects empathy toward robots. In: Proceedings of the 4th ACM/IEEE international conference on Human robot interaction, pp. 245–246. ACM (2009)
54. Saltiel, P., Wyler-Duda, K., D'Avella, A., Tresch, M.C., Bizzi, E.: Muscle synergies encoded within the spinal cord: evidence from focal intraspinal nmda iontophoresis in the frog. Journal of neurophysiology **85**(2), 605–619 (2001)
55. Santello, M., Baud-Bovy, G., Jörntell, H.: Neural bases of hand synergies. Frontiers in computational neuroscience **7**, 23 (2013)

56. Santello, M., Bianchi, M., Gabiccini, M., Ricciardi, E., Salvietti, G., Prattichizzo, D., Ernst, M., Moscatelli, A., Jörntell, H., Kappers, A.M., et al.: Hand synergies: Integration of robotics and neuroscience for understanding the control of biological and artificial hands. Physics of life reviews **17**, 1–23 (2016). DOI 10.1016/j.plrev.2016.02.001
57. Santello, M., Flanders, M., Soechting, J.F.: Postural hand synergies for tool use. Journal of Neuroscience **18**(23), 10,105–10,115 (1998)
58. Santello, M., Flanders, M., Soechting, J.F.: Patterns of hand motion during grasping and the influence of sensory guidance. Journal of Neuroscience **22**(4), 1426–1435 (2002)
59. Schafer, R.W.: What is a savitzky-golay filter?[lecture notes]. IEEE Signal processing magazine **28**(4), 111–117 (2011). DOI 10.1109/msp.2011.941097
60. Schäling, B.: The boost C++ libraries. Boris Schäling (2011)
61. Scholz, J.P., Schöner, G.: The uncontrolled manifold concept: identifying control variables for a functional task. Experimental brain research **126**(3), 289–306 (1999). DOI 10.1007/s002210050738
62. Stratmann, P., Lakatos, D., Albu-Schäffer, A.: Neuromodulation and synaptic plasticity for the control of fast periodic movement: Energy efficiency in coupled compliant joints via pca. Frontiers in neurorobotics **10** (2016). DOI 10.3389/fnbot.2016.00002
63. Thakur, P.H., Bastian, A.J., Hsiao, S.S.: Multidigit movement synergies of the human hand in an unconstrained haptic exploration task. Journal of Neuroscience **28**(6), 1271–1281 (2008). DOI 10.1523/jneurosci.4512-07.2008
64. Todorov, E., Ghahramani, Z.: Analysis of the synergies underlying complex hand manipulation. In: Engineering in Medicine and Biology Society, 2004. IEMBS'04. 26th Annual International Conference of the IEEE, vol. 2, pp. 4637–4640. IEEE (2004)
65. Tresch, M.C., Jarc, A.: The case for and against muscle synergies. Current opinion in neurobiology **19**(6), 601–607 (2009)
66. Tresch, M.C., Saltiel, P., Bizzi, E.: The construction of movement by the spinal cord. Nature neuroscience **2**(2), 162–167 (1999)
67. Turvey, M.T.: Action and perception at the level of synergies. Human movement science **26**(4), 657–697 (2007)
68. Villani, L., Ficuciello, F., Lippiello, V., Palli, G., Ruggiero, F., Siciliano, B.: Grasping and control of multi-fingered hands. In: Advanced Bimanual Manipulation, pp. 219–266. Springer (2012). DOI 10.1007/978-3-642-29041-1_5
69. Vinjamuri, R., Sun, M., Chang, C.C., Lee, H.N., Sclabassi, R.J., Mao, Z.H.: Temporal postural synergies of the hand in rapid grasping tasks. IEEE Transactions on Information Technology in Biomedicine **14**(4), 986–994 (2010)
70. Xu, K., Liu, H., Du, Y., Zhu, X.: Design of an underactuated anthropomorphic hand with mechanically implemented postural synergies. Advanced Robotics **28**(21), 1459–1474 (2014)